Bridging Ab Initio Molecular Dynamics and a Semiclassical Grand Canonical Scheme for the Electric Double Layer of the Pt(111)/Water Interface

Jun Huang,[†,‡] Yufan Zhang,[‡] Mengru Li,[†] Axel Groß,[*,†,¶] and Sung Sakong[*,†]

†Institute of Theoretical Chemistry, Ulm University, 89081 Ulm, Germany

‡IEK-13, Forschungszentrum Jülich, 52425 Jülich, Germany

¶Helmholtz Institute Ulm (HIU), Electrochemical Energy Storage, 89069 Ulm, Germany

E-mail: axel.gross@uni-ulm.de; sung.sakong@uni-ulm.de

Abstract

The theoretical modeling of metal/water interfaces centers on an appropriate electric double layer (EDL) configuration under grand canonical conditions. In principle, ab initio molecular dynamics (AIMD) simulations would be the appropriate choice for treating the competing water-water and water-metal interactions and explicitly considering the atomic and electronic degrees of freedom. However, this approach only allows simulations of relatively small canonical ensembles for limited simulation time. On the other hand, computationally efficient semiclassical approaches can treat the EDL model based on a grand canonical scheme by averaging the microscopic details. Thus, an improved description of the EDL can be obtained by combining AIMD simulations and semiclassical methods based on a grand canonical scheme. By taking the Pt(111)/water interface as an example, we present a joint effort to evaluate the electric field, water configuration, and double layer capacitance. Furthermore, we will discuss how the combined merits of the approaches can contribute to advances in EDL theory.

Introduction

As our society is on the course toward a sustainable energy economy by embracing batteries, fuel cells, and electrolyzers for energy storage and conversion, electrochemistry has become a vibrant field of research. Among various rapidly developing research fronts of electrochemistry, the electric double layer (EDL) is of particular fundamental interest and importance.[1–5] Although the EDL is an essential part of any electrochemical cell, it is notoriously difficult to assess in experiment and theory. The grand challenge for experimental studies is separating the weak EDL signal from the dominant background of the contacting solid and bulk solution phases and determining the local properties at the interface. Measurements of EDL properties have often a considerable uncertainty and in some instances, it is not easy to determine even its basic properties such as the differential capacitance.[6–9]

On the theory side, the main difficulties stem from the fact that the EDL is a complex

nano-scale open system with the electrode potential as a control parameter. The EDL often embraces a solid-phase electrode and a liquid-phase electrolyte. Thus, energetically highly degenerate configurations due to the liquid nature of the electrolyte represent the primary feature of the EDL structure. In addition, the EDL is a grand-canonical system; a seamless exchange of electron and ion species occurs between the interface and reservoirs. The first attempt to model the EDL was the Helmholtz model in 1879,[10] in which the EDL is viewed sketchily as a planar plate capacitor. Afterward, various classical EDL models have been developed in the past century, refining the description by adding new structural components, such as the Stern layer,[11] the inner and outer Helmholtz planes,[12] and quantum effects, such as the electron spillover.[1,13] However, a complete atomistic description of the interfaces and EDL is still beyond grasp.

The EDL is macroscopically charge-neutral, i.e., the charges of ionic cores and electrons are overall balanced. The optimal electron rearrangement in the EDL leads to a local polarization, e.g., the formation of ionic species, polarized water molecules, and interface dipoles. The classical approaches treat only the local polarization as distribution functions, whereas ab initio methods derive them directly from atomic configurations and electron distribution. A natural choice of parameter-free atomistic EDL modeling is, thus, density functional theory (DFT) calculations because they combine quantum chemical reliability with numerical efficiency. Based on adequately selected interface configurations, DFT can faithfully model the EDL and describe the fundamental structural and electronic properties, including the potential of zero charge (pzc), the double-layer capacitance (C_{dl}), and the surface charging relations.[14–24] However, there are practical and fundamental difficulties in DFT-based methods. Firstly, the thickness of the EDL is usually larger than one nm, which prevents modeling the whole EDL using DFT. Secondly, the liquid nature of the electrolyte necessitates an extensive statistical sampling to get meaningful thermodynamic properties, which requires computationally demanding ab initio molecular dynamics (AIMD) simulations in practice. Finally, a generally accepted grand canonical scheme is still missing. Of course, a

model with sufficiently many particles can mimic the grand canonical system, but it is computationally impractical, and since the EDL model treats a half cell of the cell, the change of the electrode potential still requires a simultaneous variation of the numbers of electrons and ionic species.

Several approximate schemes combining DFT with other methods with varying levels of sophistication have been developed, including implicit solvent methods and electrified electrodes with a compensating ion distribution in the EDL based on the Boltzmann distribution due to technical and computational limitations.[25–31] Of course, hybridizing atomistic structures and distribution functions has been proven to be rather useful and is widely accepted. However, the relationship between a microstate and thermodynamic average functions at the interfaces is largely unknown. Therefore, at the current stage, it is desirable to compare and bridge ab initio canonical models and approximate grand canonical models.

We adopt a semiclassical model developed in Refs.[32–34] to treat the EDL within a grand canonical scheme. The corresponding atomistic EDL properties are sampled along AIMD trajectories calculated using a couple of explicit ions in thin water film on the metal electrode.[9,14–16,18–22,35–44] Both EDL models are about to be compared in terms of inner potential, solvent orientation, and surface charging behaviors for the Pt(111)/water interface. We will identify the agreements and differences between the methods and connect the numerical results to experimentally accessible properties, e.g., surface charge and work function. The comparison can provide helpful insights into strengths and weakness of both methods and is instrumental to develop an improved framework that combines semiclassical and DFT methods.

Grand potential of the semiclassical EDL model

The primary task of the grand canonical modeling is to construct the grand potential Ω of the EDL, which is transformed from the Helmholtz free energy F via,

$$\Omega = F - \sum_l N_l \tilde{\mu}_l = \int (f - \sum_l n_l \tilde{\mu}_l) dr^3 = \int g dr^3, \tag{1}$$

where N_l and $\tilde{\mu}_l$ are the number and electrochemical potential of the considered charge species, respectively. We treat the interactions between charged particles with charge density functionals and assume that the Helmholtz energy density f is known for all charge species in terms of density n_l for simplicity and computational efficiency. Then, the variational analysis of the grand potential density $g[\{n_l\}]$ leads to differential equations in terms of the inner potential ϕ and valence electron density n_e,

$$\frac{\partial g}{\partial \phi} - \nabla \frac{\partial g}{\partial \nabla \phi} = \frac{\partial g}{\partial n_e} - \nabla \frac{\partial g}{\partial \nabla n_e} = 0. \tag{2}$$

The charge species in the EDL include cationic cores (denoted by the subscript cc in the following) and valence electrons e in the electrode and cations c and anions a in the electrolyte to construct the grand potential. We assume that the valence electrons in the electrode can be separately treated and describe the valence electrons quantum mechanically using the orbital-free DFT theory of the inhomogeneous electron gas.[45–47] Meanwhile, the ionic species in the electrolyte are treated classically at the mean-field level, taking into account Coulomb interactions, ion size effects, and the nonlinear polarization of solvent molecules. The inner potential ϕ, determined by charge distributions across the interface, corresponds to the one-electron potential within DFT calculations and is derived from a grand potential within the semiclassical approach. The inner potential is continuous across the whole EDL.

We arrange the Helmholtz free energy into three parts and identify the energy density

forms of each contribution: the valence electrons in the electrode F_Q, the electrostatic effects of the charge species and solvent molecules in the whole EDL F_C, and interactions (non-electrostatic ones) between valence electron and classical charged particles at the interface F_I, i.e., $F = \sum_i F_i = \sum_i \int f_i dr^3$ for $i = Q, C, I$.

The valence electron contributions in the electrode F_Q consists of the kinetic energy of non-interacting electrons T_{ni} and the exchange-correlation energy U_{XC}. We describe the kinetic energy density t_{ni} from the Thomas-Fermi-Weizsäcker theory and the exchange-correlation energy densities u_X and u_C from the PBE functional,

$$f_Q = t_{ni} + u_X + u_C. \tag{3}$$

The energy densities are functionals $t_{ni}[n_e]$, $u_X[n_e]$, $u_C[n_e]$ of electron density n_e, optimized together with other charge species in the grand potential as we will discuss below. We will not treat the valence electron entropy explicitly. By employing the kinetic energy density, the computational efficiency becomes much higher than the conventional Kohn-Sham approach, but the applicability for the electrode/electrolyte interface is still an open question. The detailed forms of the energy densities are in Table S1.

The electrostatic effects F_C of charge species include the electrostatic energy of charged particles, the self-energy of the electric field, the dipole energy of solvent molecules, and the entropy of particles, i.e., $f_C = u_{es} + u_{self} + u_{dip} + f_{ST}$. The electrostatic energy density of charge species in the EDL is

$$u_{es} = \sum_{l=cc,e,a,c} n_l q_l \phi, \tag{4}$$

with the charge density n_l and corresponding charge q_l. For example, the charges q of valence electrons and ionic cores in the electrode are $-e_0$ and e_0, respectively. The energy density of the self-energy $u_{self} = -\frac{\epsilon_0}{2}(\nabla\phi)^2$ is obtained from the Hubbard–Stratonovich transformation of particle-particle interactions with the optical permittivity ϵ_0. The dipole energy of solvent molecules is estimated by the coupling between local electric field $E = -\nabla\phi$ and dipole

moment of solvent p_s,

$$u_{dip} = -\frac{1}{\beta} \ln \frac{\sinh(\beta p_s |E|)}{\beta p_s |E|}, \tag{5}$$

with the inverse thermal energy $\beta = 1/k_B T$. The entropy of ionic species and solvent molecules f_{ST} is estimated by ideal gas expressions for each species

$$f_{ST} = \sum_{l=a,c,s} \frac{n_l}{\beta} (\ln(n_l \Lambda_l^3) - 1) + \Phi_{ex}(\{n_l\}), \tag{6}$$

with the thermal wavelength of particles Λ_l. Φ_{ex} accounts for the excess Gibbs free energy compared to the ideal gas system.

In addition to the electrostatic interactions, we consider short-range interactions at the interface F_I. We introduce a hard sphere type repulsive interaction u_{rep} preventing the ionic and solvent particles from penetrating into the electrode region using an empirical relation,

$$u_{rep} = \sum_{l=a,c,s} n_l w_{1,l} = \sum_{l=a,c,s} n_l w_{0,l} \left(\frac{\sigma_{1,l}}{z\theta(z) + \sigma_{2,l}} \right)^6, \tag{7}$$

with force constants $w_{0,l}$, the distance from the upper edge of the electrode z, and the Heaviside function $\theta(z)$. By selecting the distance parameters $\sigma_2 << \sigma_1$, the repulsive interaction becomes huge inside of the electrode ($z < 0$), which ensures a near-zero probability of the ionic particles and solvent molecules in the electrode region. The repulsive interaction rapidly decreases outside of the electrode and becomes negligible in the bulk electrolyte with a large z.

We account for a bilinear interaction between particles in the electrolyte and valence electrons, $w_{2,l} n_l n_e$ for $l = a, c, s$. The relation represents a repulsive or attractive interaction between the particles in the electrolyte and the valence electrons. Then, the energy density can represent the specific adsorption of ionic species and solvent molecules on the electrode.

Then, the energy density f_I is

$$f_I = u_{rep} + \sum_{l=a,c,s} w_{2,l} n_l n_e. \tag{8}$$

The grand potential density g is constructed by combining all listed free energy densities f and electrochemical potentials $\tilde{\mu}$. Then, the variational analysis of Eq. 2 leads to the Poisson equation,

$$-\nabla[\epsilon_{eff}\nabla\phi] = \sum_{l=cc,e,a,c} n_l q_l, \tag{9}$$

with an effective dielectric constant of the solvent,[48]

$$\epsilon_{eff} = \epsilon_0 + \frac{n_s p_s}{|E|}\left(\coth(\beta p_s|E|) - \frac{1}{\beta p_s|E|}\right). \tag{10}$$

Alternatively, the variational analysis in terms of the valence electron density n_e or particle density n_l ($l = a, c, s$) leads to another set of differential equations in terms of n_e,

$$\nabla\left[\frac{\partial f_Q}{\partial\nabla n_e}\right] = \frac{\partial f_Q}{\partial n_e} + \sum_{l=a,c,s} w_{2,l} n_l - e_0\phi - \tilde{\mu}_e, \tag{11}$$

and in terms of n_l,

$$w_{1,l} + w_{2,l} n_e + \frac{\ln(n_l\Lambda_l^3)}{\beta} + \frac{\delta\Phi_{ex}}{\delta n_l} - \tilde{\mu}_l \tag{12}$$

$$= -q_l\phi \quad \text{for } l = a, c,$$

$$= \frac{1}{\beta}\ln\frac{\sinh(\beta p_s|E|)}{\beta p_s|E|} \quad \text{for } l = s.$$

By applying the constraints and boundary conditions to the differential equations, the EDL properties (ϕ, n_e, and n_l) are optimized. We list further details of the variational analysis in the SI.

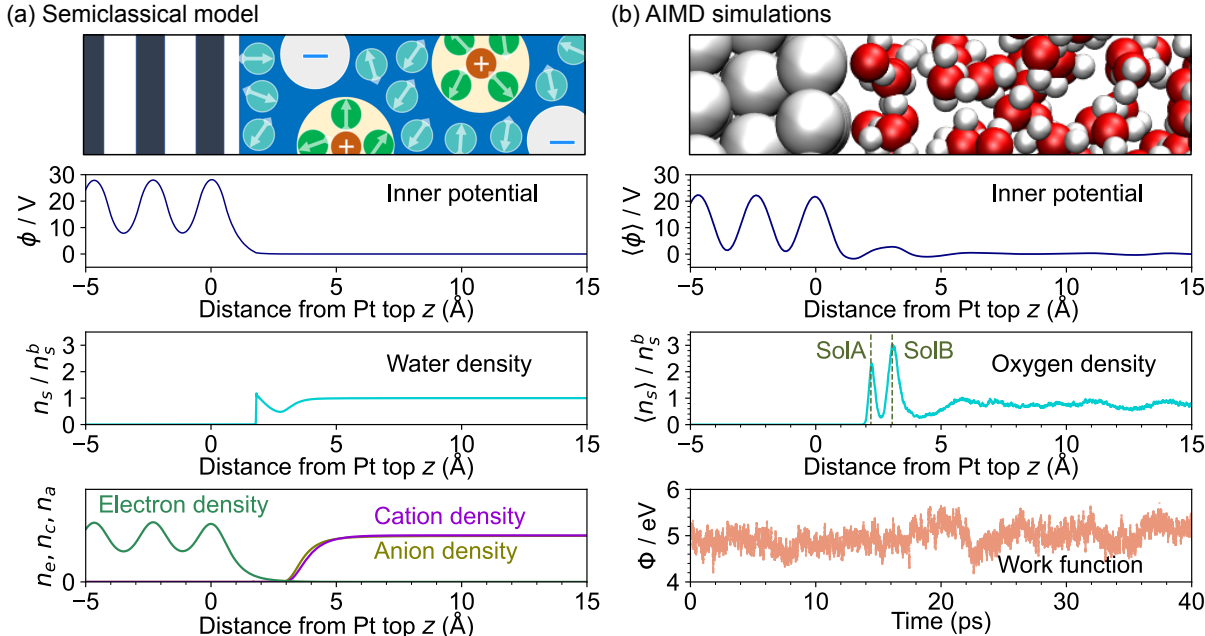# Modeling EDL structures from semiclassical and AIMD methods

Figure 1: System setup and typical results in the semiclassical model (a) and AIMD simulation (b). The subplots show the EDL configurations, distributions of the inner potential, and the water molecule density normalized to the bulk value in both methods. In the lowest panel of (a), the metal electron density is normalized to the density of the metal cationic cores. The cation and anion densities are normalized to their bulk values. The lowest panel of (b) shows a trajectory of work function at the pzc in the AIMD simulations.

We employ a one-dimensional array of layers to model the EDL structure in the semiclassical model. By assuming an averaged grand potential density in each layer, we treat an effective grand potential g_z, i.e., $\Omega = \int g_z dz$. The semiclassical model in Fig. 1(a) consists of the atomic cores modeled by a constant positive charge with a core radius. The averaging of the core densities in the layer leads to an one-dimensional positive charge distribution along the coordinate z. The atomic structure of the electrode determines the width of layers a_{mc}, spacing between layers $2t$, and spacing t between the electrode and electrolyte parts. We note that the densities of water and ionic species are allowed to get finite values in the spac-

ing t because the model treats continuously varying EDL properties from the metal phase to the bulk solution. More importantly, distributions of the inner potential, the metal electron density, the ion densities, and the solvent molecule density are optimized as a function of the electrode potential.

Figure 1(a) demonstrates the semiclassical results at the pzc. The inner potential shows strong variation around the cationic metal cores while it is smooth in the solution phase. The potential gradually decreases from the metal phase to the solution phase at the interface. The particle densities of water molecules and ions are derived by solving Eqs. 11 and 12. We note that a large value for the repulsive interactions u_{rep} of Eq. 7 ensures the separation between electrode and solution phases, as shown by the number density of ions and water molecules in the two lower panels of Fig. 1(a). Outside the metal phase, u_{rep} immediately vanishes, and water molecule density approaches the bulk liquid value. Interestingly, a suitable choice of u_{rep} allows a peak formation at around $z = 1.75$ Å. In the semiclassical approach, the water density peak at the interface results from a subtle balance of the bilinear interaction f_I, found in AIMD simulations in Fig. 1(b). The lowest panel of Fig. 1(a) demonstrates the cation and anion densities at the pzc. The total number of cations and anions (integrals of ion densities) in the EDL should be the same at the pzc. However, the density distributions do not necessarily overlap in the EDL. We note that the electrolyte is slightly negatively polarized at $z < 5$ Å, a response to the oscillations in the electrode. The semiclassical model captures the spillover of electrons from the electrode. Namely, a portion of electrons spreads into the solution compartment with an approximately exponentially decaying density profile. The optimized inner potential and electron density show a similar distribution, consisting of a drop at the electrode surface, a significant part of the work function change. We note that the spatial gap between the metal and solution phases also influences the potential drop at interfaces and, consequently, the pzc.

AIMD trajectories were obtained by solving the generalized Langevin equation at 298 K up to 40 ps with a time step of 1 fs. The energies and forces were computed on a five-layer

10

Pt(111) slab interfaced with 144 water molecules in a 6×6 surface unit cell, under the conditions of the pzc according to Trasatti,[49] using the Vienna ab initio simulation (VASP) package. We have prepared positively and negatively charged conditions by adding an H atom to or removing it from the water film, leading to an electron transfer from and to the Fermi level, respectively, and resulting in hydronium or hydroxyl formation in the solution. Effectively, the net charge of the electrode was modulated by varying the pH in the water film which then became compensated by the resulting explicit counter ion in the water film. Within the AIMD approach, each snapshot of the trajectories represents a microstate of the canonical ensemble. Besides the canonical sampling along each trajectory, we perform a grand canonical sampling by selecting snapshots from all considered trajectories for specified work functions, irrespective of the number of H atoms in the water film, as suggested by Rossmeisl et al.[50,51] We refer to our previous works for further technical details.[39,40]

Figure 1(b) shows a snapshot of the AIMD simulations and sampled properties at the pzc. The work function along the canonical trajectories in the lower panel shows a sizeable thermal fluctuation. The standard deviation is around 0.2 eV for all presented trajectories. The inner potential and water distribution in Fig. 1(b) are averaged over the snapshots at the pzc. We note the densely packed water layers labeled by SolA and SolB at the interface, which are not explicitly addressed within the semiclassical approach. As shown below, the two water layers result in a hump of the inner potential.

Inner potential of the EDL

Figure 2 compares the averaged inner potentials derived from the AIMD and semiclassical methods. Within the AIMD simulations, the EDL charging is realized by removing/adding a hydrogen atom in the water layer, resulting in a hydroxyl anion (OH^-) or a hydronium cation (H_3O^+) formation, respectively, as shown in the upper panel of Fig. 2(b). We align the vacuum levels of ϕ in the three trajectories and display ϕ with respect to the bulk electrolyte
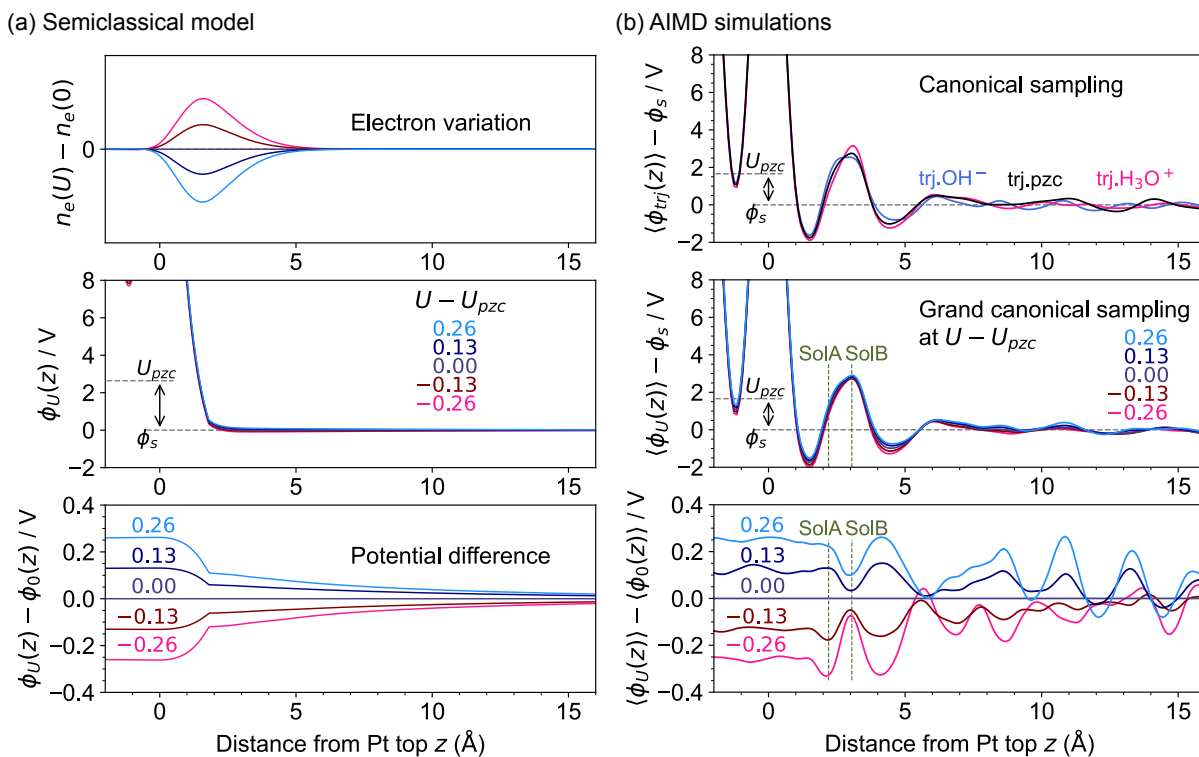
Figure 2: The local potential of the EDL calculated from (a) the AIMD simulations and (b) the semiclassical model. In the AIMD simulations, three cases, including a base case, a positively charged case with a OH^- in solution, and a negatively charged case with a hydronium ion in solution, are compared. In the semiclassical model, five electrode potentials referenced to the potential of zero charge are compared.

value ϕ_s. In the semiclassical approach, we assign the U_{pzc} as the potential where the net ionic charge in the solution is zero.

The AIMD potentials $\langle \phi_{trj}(z) \rangle$ derived from canonical sampling in the upper panel of Fig. 2(b) show relatively strong oscillations and cross each other in the EDL region. To address the results comparable to the semiclassical model, we construct the thermodynamic ensemble using all considered AIMD trajectories, trj.pzc, trj.H_3O^+, trj.2H_3O^+, and trj.OH^-. Then, in the spirit of the grand canonical ensemble,[52] we select all configurations according to their work function and perform the average for all trajectories within an interval around five selected values of the electrode potential U, as shown in the middle panel of Fig. 2(b). We note an oscillation of the potential ϕ_U in the solvation layer compared to the smoothly varying semiclassical potential in the grand canonical samplings. The oscillating structure results from structured water molecules at the interface. As shown in Section , the metal-water interactions govern the water structures in the EDL, whose configurations are associated with the interface dipole formation.[18,39] Subsequently, it causes a reduced difference between the electrode potential U_{pzc} and the level of the bulk liquid water ϕ_s.[53,54] As suggested by an early model study addressing the relationship between work function change and metal-water interaction strength,[55] the interactions at the interface determine the absolute position of U_{pzc}.

The change in the charge of the electrode caused by the variation of the electrode potential is located in the region -1 to 5 Å away from the top Pt layer because of the quantum mechanical nature of electrons, as shown in the upper panel of Fig. 2(a). The semiclassical model captures the electron spillover by treating the electron distribution quantum mechanically through Eq. 3. The semiclassical and AIMD results show that the charge change occurs where the structured water molecules exist, as depicted in the middle panels of Figs. 2(a) and (b). The excess and depletion of charge in the solvation layer influence the chemical interactions of the water molecules and adsorbed ionic species.

The lowest panels of Fig. 2 show the potential shift at five different electrode potentials.

The potentials inside the electrode are consistent in both methods. The semiclassical method predicts a smooth potential change from the electrode to the electrolyte. It does not yield any oscillatory structure in the electrolyte as it assumes a smooth and continuous water distribution and a linear response of the water orientation to the electric field. In contrast, the AIMD simulations show that water molecules directly interacting with the electrode can influence the inner potential at the interface, whose structures are less sensitive to the electric field change. In the lowest panel of Fig. 2(a), the semiclassical method shows that the potential change in the bulk region is extended over a long-range (10 nm) until the counterion distribution fully compensates for the electrode charging. Such an extensive distribution is difficult to reproduce within the AIMD simulations because of the limited thickness of the water layer. Consequently, the counterion distribution in the AIMD simulations is limited to a relatively short range (1 nm). Thus, AIMD simulations might not be able to fully capture the thermodynamic average of the counterion distribution.

Water structures in the EDL

In this section, we will now address the explicit configuration of the water molecules in the EDL, as derived from AIMD simulations and the semiclassical model. The local water configuration in the EDL is analyzed by focusing on the angle between the water dipole p_s through the derived electric field E. As illustrated in Fig. 3(a), the θ represents the angle between the water bisection vector and inward normal to the electrode surface. In the semiclassical model, the contributions are included through the dipole energy u_{dip} in Eq. 5 and the ensemble average of $\cos\theta$ is given by

$$\langle \cos\theta \rangle = \coth\beta p_s E - \frac{1}{\beta p_s E}, \tag{13}$$

with the Boltzmann constant k_B. The asymptotic behaviors of the angular distribution for a vanishing electric field $E \to 0$ yields a random orientation of the water dipole $\langle \cos\theta \rangle \to 0$.
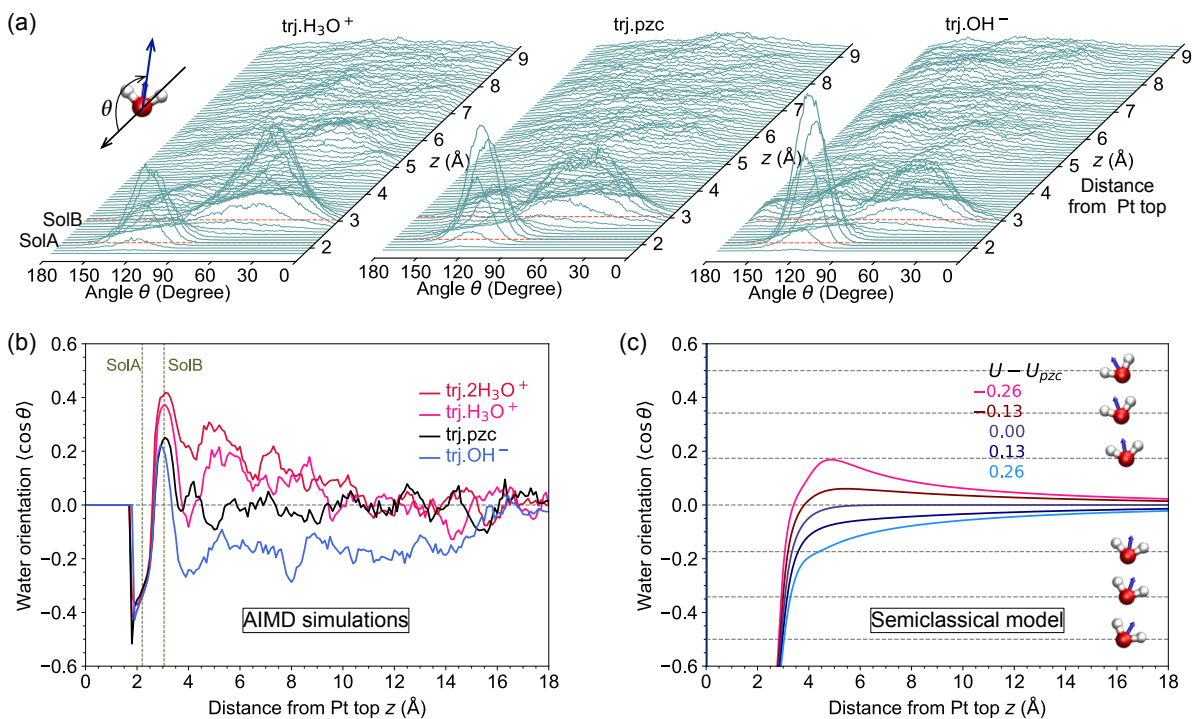
Figure 3: Orientation of water molecules near the metal surface in the AIMD simulations (a, b) and the semiclassical model (c). In (b) and (c), $\langle \cos\theta \rangle$ represents the ensemble average value of $\cos\theta$ with θ being the angle between the water dipole orientation (pointing from O towards H) and the inward normal direction perpendicular to the metal surface.

For positive and negative electric fields, the value changes from -1 to 1. Thus, in practice, the structural arrangement of the water molecules is determined by the optimized inner potential ϕ and subsequently determined field $E = -\partial_z \phi$ within the semiclassical method. The expression of water orientation in Eq. 13 can be further refined, for example, by taking into account the chemisorption of water molecules (see Eq. (16) in Ref.[56]). In contrast, from the AIMD simulations, the water structures can be analyzed based on snapshots of the considered trajectories.

Figure 3(a) shows the distribution of water orientations as a function of the distance from the Pt electrode z derived from AIMD simulations for three different surface charging situations. In the solvation layer ($z < 4$ Å), there are pronounced peaks in the distribution visible whereas no distinguishable peaks appear above the solvation layer ($z > 4$ Å). The peak height reflects the abundance of the water molecules aligned in the corresponding orientation. Note that along the trajectory trj.OH$^-$, i.e., for a more positively charged Pt surface, the peaks in the angular distribution become more pronounced.

As shown in Fig. 3(a), in the SolA region for $z < 2$ Å, the water orientation $\langle \cos \theta \rangle$ is strongly peaked in the negative direction, and the peak heights are almost independent of the conditions of the AIMD simulations. The negative peaks in the SolA region indicate that the preferential orientation of molecules is with the oxygen atom towards the surface, or in other words, with the OH groups pointing outwards, independent of the charging of the surface. In the SolB region, the O-H bonds of the water molecules point in the opposite direction toward the electrode. However, the preferential orientation becomes less pronounced for more positively charged surfaces. Still, the OH orientation is always toward the electrode. By comparing the AIMD simulations in Fig. 3(b) to the semiclassical method in (c), we note a poor agreement. The semiclassical method only accounts for the response of the water molecules to the electric field, while AIMD simulations take into account both water-metal and water-water interactions. Consequently, within the semiclassical approach, the detailed solvation water configurations rely on the mean-field water-water interactions and are not

adequately reproduced due to the lack of proper metal-water interactions. Still, in Fig. 3(c), the water molecules in the SolA region properly orient outward from the electrode for all electrode potentials caused by the intrinsic electric field of the metal. However, the angle is overestimated compared to the AIMD simulations because the Pt-water interaction is mainly operative for the water molecules in the SolA region but not for the water molecules further away. In addition, the semiclassical method predicts a more significant variation of water orientation at the interface than AIMD simulations. Strong enough metal-water interactions dictate the water configurations at the interface, and the influence of the local electric field becomes less significant in the solvation layer.

Under the pzc condition, the polarization of ionic species rapidly vanishes above the solvation layer (above 4 Å), and the electrostatic potential corresponds to the bulk liquid level ϕ_s. The flat local potential leads to a vanishing electric field $-\nabla\phi \to 0$, which is valid for the uncharged electrochemical electrolyte/electrode interfaces in equilibrium. The average $\cos\theta$ of randomly distributed water molecules in the bulk liquid phase becomes zero. The semiclassical approach, see the black line in Fig. 3(c), reflects this random water orientation above 5 Å at the pzc. In the AIMD simulations, the selection of an ion-free water film constitutes the pzc condition. Although the interface dipole formation negatively polarizes the electrode, the influence of the dipole field is limited to the solvation layer region and does not affect the water orientation in the bulk region. In the bulk water region, the average water orientation (the black line in Fig. 3(b)) fluctuates around zero.

By polarizing the EDL and subsequently creating the electric field, the water molecules tend to orient upward/downward from the electrode at a potential below/above the pzc. The ordered tendency of water orientation exists up to the distance where the polarization occurs, and water molecules recover a random distribution beyond the EDL. Both AIMD and semiclassical methods reproduce the tendency correctly in the bulk liquid area as shown in the positive values of the red and pink lines and the negative values of the blue line in Figs. 3(b) and (c). This corresponds to the relatively flat angular distribution in trj.pzc for

17

the distance beyond 4 Å in Fig. 3(a), while small hills on the right and left sides of the plains of trj.H_3O^+ and trj.OH^- in Fig. 3(a), respectively. Of course, the AIMD sampling is performed in a limited simulation time and shows fluctuations and the influence of the initial position of ion species. Especially slowly drifting OH^- is found around the initial position for the simulation time. However, the results are in qualitative agreement with the grand canonical scheme from the semiclassical model.

Structural differences between AIMD and semiclassical simulations occur in the solvation layer for distances below $z < 4$ Å, where the water-metal interaction dominates the water configuration.[57] The angular distribution of the water molecules in the SolB region does depend on the electrode potential, but $\langle\cos\theta\rangle$ always remains positive, indicating a preferential orientation of the water molecules with their hydrogen atoms pointing towards the surface. In contrast, the semiclassical model assumes a bulk-like random orientation. Hence it is limited to capturing the preferential orientation of the water molecules in the SolB region.
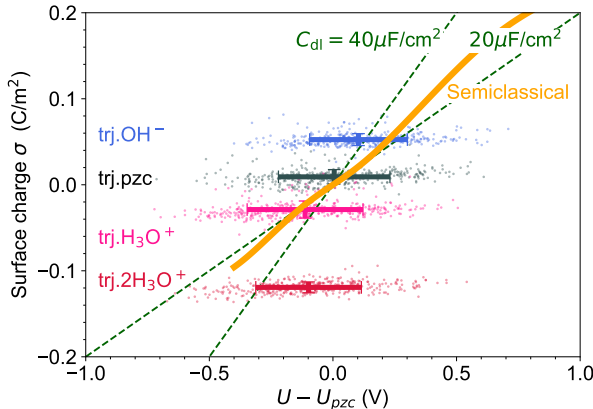
Differential double layer capacitance

Figure 4: Surface charging relation calculated from the semiclassical model. The two dashed lines correspond to $\sigma = C_{dl}(U - U_{pzc})$ with a double layer capacitance of 20 and 40 $\mu F/cm^2$, respectively. The error bars correspond to the AIMD results where the surface charge density σ is fixed while the potential varies due to fluctuations in the water configurations.

The charge polarization of the electrode is defined as,

$$\sigma = \int_{-\infty}^{\infty} (n_{mc}(z) - n_e(z))e_0 dz, \tag{14}$$

$$= -\int_{-\infty}^{\infty} (n_c(z) - n_a(z))e_0 dz, \tag{15}$$

where n_{mc} and n_e are the charge densities of metal cationic cores and electrons, respectively. e_0 represents the elementary charge. As the entire EDL is electroneutral, the surface charge polarization σ must be balanced by the net charge stored in the double layer. Within the semiclassical approach, charged species (cationic metal cores, valence electrons, anions, and cations) can be separately treated. However, within quantum chemistry simulations, the electrons are delocalized, and there is no clear way to separate the electrons and attribute them either to the electrode or the electrolyte. Therefore, we rely on a charge partition scheme to analyze the charge polarization within AIMD simulations, as discussed previously.[39] We evaluate the charge partitioning for every 100th step, i.e., in total, for 400 snapshots along each trajectory.

Within the semiclassical approach, the pzc corresponds to the electrode potential at $\sigma = 0$. We consider the excess free electrons as the deviation from the charge distribution at the pzc. As discussed above, the added or removed charge is distributed across the solvation layer, and considering only the polarization in the Pt atoms cannot capture the total surface charge. Therefore, we also take the polarization of the water molecules within the IHP into account. In practice, since the IHP is dynamically defined at each time step, we monitor the water polarization by determining the position where the water polarization becomes constant as a function of the distance from the surface. In Fig. 4, the surface charge σ derived from the AIMD simulations (dots) and the semiclassical method (solid orange line) are displayed. The dashed guidelines represent double-layer capacitances of 20 and 40 $\mu F/cm^2$, corresponding to typical experimental findings.[58]

According to Fig. 4, σ increases monotonically from negative to positive values as U in-

creases. The differential double-layer capacitance can be calculated from the surface charging curve by taking the derivative of the surface charge σ with respect to the electrode potential U, namely $C_{\mathrm{dl}} = \partial\sigma/\partial U$. The modest variation of the surface charge along the single trajectories indicates that the orientation and alignment of the water molecules mainly influence the variations on the work function, as already demonstrated using the bilayer models.[55] Furthermore, the distributions of the surface charges of the considered trajectories are well separated from each other. The AIMD sampling in Fig. 4 shows a broad distribution of the work functions but a relatively well-defined surface charge for each trajectory. Thus, the grand canonical sampling is inapplicable to analyze the well-separated surface charges from each other, and the selecting appropriate water configurations is essential to determine the proper electrode potential.

An ion-free water film corresponds to the water configurations at the pzc, as suggested by Trasatti.[49] A slight variation of the water film by adding one hydronium or OH^- ion leads to a shift of surface charge and the work function. The estimated capacitances from AIMD and semiclassical methods are in good agreement with the experiment.[58] However, as the crimson dots in Fig. 4 indicate, the work function is outside of the range expected from experiments for the water film with two hydronium ions. The fluctuation of the work function is a consequence of the limited size of the simulation cell. A larger surface unit cell reduces the variation in the work function along the trajectory, as shown in Fig. 10 of Ref.[3] At electrochemical electrolyte/electrode interfaces, the solvation water structure depends on the electrode charge, the presence of adsorbates,[18,59] and ion distributions near the surface. All related elements must be optimized in a grand canonical fashion. An adequately tailored structure based on a grand canonical scheme allows reliable statistical sampling for a specific electrochemical condition.

Conclusion

In this study, we have addressed the structure of the electric double layer (EDL) using two different approaches: ab initio molecular dynamics (AIMD) simulations and a semiclassical model. In practice, we note a good agreement between the two applied methods. Since electrostatic interactions primarily govern the EDL properties, the semiclassical model can provide a reasonable description within a grand canonical scheme by accounting for essential polarization density distributions. However, the fine details of the interface structure found in AIMD simulations require more than the proper selection of boundary conditions at the bulk phase electrode and electrolyte. An explicit consideration and proper parametrization of metal electron-solvent particle interactions are necessary for a more advanced description, hence the semiclassical model requires further improvements to capture the findings from the AIMD simulations. The large spread of the sampled properties from AIMD simulations indicates that the method needs a larger simulation cell or a longer sampling time to derive more concrete values. An attempt using machine-learning based force fields with DFT accuracy may help to overcome the computational and technical limitations.[44,60–62] However, an accurate description of electrochemical environments within AIMD simulations requires adequately tailored atomic configurations. Therefore, the semiclassical method will retain its importance as a reference for the AIMD simulation. Thus, feed and feedback between the semiclassical and AIMD methods are essential for future developments of EDL modeling.

Acknowledgements

References

(1) Schmickler, W. Electronic Effects in the Electric Double Layer. *Chem. Rev.* **1996**, *96*, 3177–3200.

(2) Groß, A.; Sakong, S. Modelling the electric double layer at electrode/electrolyte interfaces. *Curr. Opin. Electrochem.* **2019**, *14*, 1–6.

(3) Groß, A.; Sakong, S. Ab Initio Simulations of Water/Metal Interfaces. *Chem. Rev.* **2022**, *122*, 10746–10776.

(4) Sakong, S.; Huang, J.; Eikerling, M.; Groß, A. The structure of the electric double layer: Atomistic versus continuum approaches. *Curr. Opin. Electrochem.* **2022**, *33*, 100953.

(5) Wu, J. Understanding the Electric Double-Layer Structure, Capacitance, and Charging Dynamics. *Chem. Rev.* **2022**, *122*, 10821–10859.

(6) Gómez, R.; Climent, V.; Feliu, J. M.; Weaver, M. J. Dependence of the Potential of Zero Charge of Stepped Platinum (111) Electrodes on the Oriented Step-Edge Density: Electrochemical Implications and Comparison with Work Function Behavior. *J. Phys. Chem. B* **2000**, *104*, 597–605.

(7) Climent, V.; Attard, G. A.; Feliu, J. M. Potential of zero charge of platinum stepped surfaces: a combined approach of CO charge displacement and N2O reduction. *J. Electroanal. Chem.* **2002**, *532*, 67–74.

(8) Martínez-Hincapié, R.; Climent, V.; Feliu, J. M. Investigation of the interfacial properties of platinum stepped surfaces using peroxodisulfate reduction as a local probe. *Electrochim. Acta* **2019**, *307*, 553–563.

(9) Li, P.; Liu, Y.; Chen, S. Microscopic EDL structures and charge–potential relation on stepped platinum surface: Insights from the ab initio molecular dynamics simulations. *J. Chem. Phys.* **2022**, *156*, 104701.

(10) Helmholtz, H. Studien über electrische Grenzschichten. *Ann. Phys. (Leipzig)* **1879**, *243*, 337–382.

(11) Stern, O. Zur Theorie der Elektrolytischen Doppelschicht. *Z. Elektrochem. Angew. P.* **1924**, *30*, 508–516.

(12) Gouy, L. G. Sur la constitution de la charge électrique à la surface d'un électrolyte. *C. R. Hebd. Seances Acad. Sci.* **1909**, *149*, 654–657.

(13) Badiali, J. P.; Rosinberg, M. L.; Vericat, F.; Blum, L. A microscopic model for the liquid metal-ionic solution interface. *J. Electroanal. Chem. Interfacial Electrochem.* **1983**, *158*, 253–267.

(14) Le, J.; Iannuzzi, M.; Cuesta, A.; Cheng, J. Determining Potentials of Zero Charge of Metal Electrodes versus the Standard Hydrogen Electrode from Density-Functional-Theory-Based Molecular Dynamics. *Phys. Rev. Lett.* **2017**, *119*, 016801.

(15) Le, J.; Fan, Q.; Perez-Martinez, L.; Cuesta, A.; Cheng, J. Theoretical insight into the vibrational spectra of metal–water interfaces from density functional theory based molecular dynamics. *Phys. Chem. Chem. Phys.* **2018**, *20*, 11554–11558.

(16) Le, J.; Cuesta, A.; Cheng, J. The structure of metal-water interface at the potential of zero charge from density functional theory-based molecular dynamics. *J. Electroanal. Chem.* **2018**, *819*, 87–94.

(17) Liu, J.; Huang, J. A mean-field model for the double layer of stepped platinum single-crystal electrodes. *J. Electroanal. Chem.* **2019**, *846*, 113136.

(18) Li, P.; Huang, J.; Hu, Y.; Chen, S. Establishment of the Potential of Zero Charge of Metals in Aqueous Solutions: Different Faces of Water Revealed by Ab Initio Molecular Dynamics Simulations. *J. Phys. Chem. C* **2021**, *125*, 3972–3979.

(19) Le, J.-B.; Fan, Q.-Y.; Li, J.-Q.; Cheng, J. Molecular origin of negative component of Helmholtz capacitance at electrified Pt(111)/water interface. *Sci. Adv.* **2020**, *6*, eabb1219.

(20) Le, J.-B.; Cheng, J. Modeling electrochemical interfaces from ab initio molecular dynamics: water adsorption on metal surfaces at potential of zero charge. *Curr. Opin. Electrochem.* **2020**, *19*, 129–136.

(21) Le, J.-B.; Cheng, J. Modeling electrified metal/water interfaces from ab initio molecular dynamics: Structure and Helmholtz capacitance. *Curr. Opin. Electrochem.* **2021**, *27*, 100693.

(22) Le, J.-B.; Chen, A.; Li, L.; Xiong, J.-F.; Lan, J.; Liu, Y.-P.; Iannuzzi, M.; Cheng, J. Modeling Electrified Pt(111)-H_{ad}/Water Interfaces from Ab Initio Molecular Dynamics. *JACS Au* **2021**, *1*, 569–577.

(23) Chen, A.; Le, J.-B.; Kuang, Y.; Cheng, J. Modeling stepped Pt/water interfaces at potential of zero charge with ab initio molecular dynamics. *J. Chem. Phys.* **2022**, *157*, 094702.

(24) Li, L.; Liu, Y.-P.; Le, J.-B.; Cheng, J. Unraveling molecular structures and ion effects of electric double layers at metal water interfaces. *Cell Rep. Phys. Sci.* **2022**, *3*, 100759.

(25) Otani, M.; Sugino, O. First-principles calculations of charged surfaces and interfaces: A plane-wave nonrepeated slab approach. *Phys. Rev. B* **2006**, *73*, 115407.

(26) Letchworth-Weaver, K.; Arias, T. A. Joint density functional theory of the electrode-

electrolyte interface: Application to fixed electrode potentials, interfacial capacitances, and potentials of zero charge. *Phys. Rev. B* **2012**, *86*, 075140.

(27) Sundararaman, R.; Goddard, W. A.; Arias, T. A. Grand canonical electronic density-functional theory: Algorithms and applications to electrochemistry. *J. Chem. Phys.* **2017**, *146*, 114104.

(28) Mathew, K.; Sundararaman, R.; Letchworth-Weaver, K.; Arias, T. A.; Hennig, R. G. Implicit solvation model for density-functional study of nanocrystal surfaces and reaction pathways. *J. Chem. Phys.* **2014**, *140*, 084106.

(29) Mathew, K.; Kolluru, V. S. C.; Mula, S.; Steinmann, S. N.; Hennig, R. G. Implicit self-consistent electrolyte model in plane-wave density-functional theory. *J. Chem. Phys.* **2019**, *151*, 234101.

(30) Melander, M. M.; Kuisma, M. J.; Christensen, T. E. K.; Honkala, K. Grand-canonical approach to density functional theory of electrocatalytic systems: Thermodynamics of solid-liquid interfaces at constant ion and electrode potentials. *J. Chem. Phys.* **2019**, *150*, 041706.

(31) Ringe, S.; Hörmann, N. G.; Oberhofer, H.; Reuter, K. Implicit Solvation Methods for Catalysis at Electrified Interfaces. *Chem. Rev.* **2022**, *122*, 10777–10820.

(32) Huang, J.; Li, P.; Chen, S. Potential of zero charge and surface charging relation of metal-solution interphases from a constant-potential jellium-Poisson-Boltzmann model. *Phys. Rev. B* **2020**, *101*, 125422–.

(33) Huang, J. Hybrid density-potential functional theory of electric double layers. *Electrochim. Acta* **2021**, *389*, 138720.

(34) Huang, J.; Chen, S.; Eikerling, M. Grand-Canonical Model of Electrochemical Double

Layers from a Hybrid Density–Potential Functional. *J. Chem. Theory Comput.* **2021**, *17*, 2417–2430.

(35) Skúlason, E.; Karlberg, G. S.; Rossmeisl, J.; Bligaard, T.; Greeley, J.; Jónsson, H.; Nørskov, J. K. Density functional theory calculations for the hydrogen evolution reaction in an electrochemical double layer on the Pt(111) electrode. *Phys. Chem. Chem. Phys.* **2007**, *9*, 3241.

(36) Groß, A.; Gossenberger, F.; Lin, X.; Naderian, M.; Sakong, S.; Roman, T. Water Structures at Metal Electrodes Studied by Ab Initio Molecular Dynamics Simulations. *J. Electrochem. Soc.* **2014**, *161*, E3015–E3020.

(37) Sakong, S.; Naderian, M.; Mathew, K.; Hennig, R. G.; Groß, A. Density functional theory study of the electrochemical interface between a Pt electrode and an aqueous electrolyte using an implicit solvent method. *J. Chem. Phys.* **2015**, *142*, 234107.

(38) Sakong, S.; Forster-Tonigold, K.; Groß, A. The structure of water at a Pt(111) electrode and the potential of zero charge studied from first principles. *J. Chem. Phys.* **2016**, *144*, 194701.

(39) Sakong, S.; Groß, A. The electric double layer at metal-water interfaces revisited based on a charge polarization scheme. *J. Chem. Phys.* **2018**, *149*, 084705.

(40) Sakong, S.; Groß, A. Water structures on a Pt(111) electrode from ab initio molecular dynamic simulations for a variety of electrochemical conditions. *Phys. Chem. Chem. Phys.* **2020**, *22*, 10431–10437.

(41) Lin, X.; Shao, A.; Hua, M.; Tian, X. A first-principles study of water adsorbed on flat and stepped silver surfaces. *Phys. Chem. Chem. Phys.* **2022**, *24*, 6803–6810.

(42) Lan, J.; Hutter, J.; Iannuzzi, M. First-Principles Simulations of an Aqueous CO/Pt(111) Interface. *J. Phys. Chem. C* **2018**, *122*, 24068–24076.

(43) Lan, J.; Rybkin, V. V.; Iannuzzi, M. Ionization of Water as an Effect of Quantum Delocalization at Aqueous Electrode Interfaces. *J. Phys. Chem. Lett.* **2020**, *11*, 3724–3730.

(44) Jinnouchi, R.; Karsai, F.; Verdi, C.; Kresse, G. First-principles hydration free energies of oxygenated species at water–platinum interfaces. *J. Chem. Phys.* **2021**, *154*, 094107.

(45) Wang, Y. A.; Carter, E. A. In *Theoretical Methods in Condensed Phase Chemistry*; Schwartz, S., Ed.; Springer, 2002; Chapter 5, pp 117–184.

(46) Gavini, V.; Bhattacharya, K.; Ortiz, M. Quasi-continuum orbital-free density-functional theory: A route to multi-million atom non-periodic DFT calculation. *J. Mech. Phys. Solids* **2007**, *55*, 697–718.

(47) Karasiev, V. V.; Trickey, S. B. In *Advances in Quantum Chemistry*; Sabin, J. R., Cabrera-Trujillo, R., Eds.; Academic Press, 2015; Vol. 71; Chapter 9, pp 221–245.

(48) Gongadze, E.; Iglič, A. Decrease of permittivity of an electrolyte solution near a charged surface due to saturation and excluded volume effects. *Bioelectrochemistry* **2012**, *87*, 199–203.

(49) Trasatti, S. Structure of the metal/electrolyte solution interface: new data for theory. *Electrochim. Acta* **1991**, *36*, 1659 – 1667.

(50) Hansen, M. H.; Rossmeisl, J. pH in Grand Canonical Statistics of an Electrochemical Interface. *J. Phys. Chem. C* **2016**, *120*, 29135–29143.

(51) Hansen, M. H.; Nilsson, A.; Rossmeisl, J. Modelling pH and potential in dynamic structures of the water/Pt(111) interface on the atomic scale. *Phys. Chem. Chem. Phys.* **2017**, *19*, 23505–23514.

(52) Nielsen, M.; Björketun, M. E.; Hansen, M. H.; Rossmeisl, J. Towards first principles

modeling of electrochemical electrode–electrolyte interfaces. *Surf. Sci.* **2015**, *631*, 2 – 7.

(53) Hörmann, N. G.; Guo, Z.; Ambrosio, F.; Andreussi, O.; Pasquarello, A.; Marzari, N. Absolute band alignment at semiconductor-water interfaces using explicit and implicit descriptions for liquid water. *Npj Comput. Mater.* **2019**, *5*, 100.

(54) Bramley, G.; Nguyen, M.-T.; Glezakou, V.-A.; Rousseau, R.; Skylaris, C.-K. Reconciling Work Functions and Adsorption Enthalpies for Implicit Solvent Models: A Pt (111)/Water Interface Case Study. *J. Chem. Theory Comput.* **2020**, *16*, 2703–2715.

(55) Schnur, S.; Groß, A. Properties of metal–water interfaces studied from first principles. *New J. Phys.* **2009**, *11*, 125003.

(56) Huang, J. Modelling of Electrocatalytic Double Layers with Refined Treatment of Metal-Water Interactions and Chemisorption. ChemRxiv, DOI:10.26434/chemrxiv-2022-fk36d-v3.

(57) Wang, Y.-H.; Zheng, S.; Yang, W.-M.; Zhou, R.-Y.; He, Q.-F.; Radjenovic, P.; Dong, J.-C.; Li, S.; Zheng, J.; Yang, Z.-L. et al. In situ Raman spectroscopy reveals the structure and dissociation of interfacial water. *Nature* **2021**, *600*, 81–85.

(58) Pajkossy, T.; Kolb, D. M. Double layer capacitance of Pt(111) single crystal electrodes. *Electrochim. Acta* **2001**, *46*, 3063–3071.

(59) Surendralal, S.; Todorova, M.; Neugebauer, J. Impact of Water Coadsorption on the Electrode Potential of H-Pt(111)-Liquid Water Interfaces. *Phys. Rev. Lett.* **2021**, *126*, 166802.

(60) Natarajan, S. K.; Behler, J. Neural network molecular dynamics simulations of solid–liquid interfaces: water at low-index copper surfaces. *Phys. Chem. Chem. Phys.* **2016**, *18*, 28704–28725.

(61) Behler, J. First Principles Neural Network Potentials for Reactive Simulations of Large Molecular and Condensed Systems. *Angew. Chem. Int. Ed.* **2017**, *56*, 12828–12840.

(62) Jinnouchi, R.; Lahnsteiner, J.; Karsai, F.; Kresse, G.; Bokdam, M. Phase Transitions of Hybrid Perovskites Simulated by Machine-Learning Force Fields Trained on the Fly with Bayesian Inference. *Phys. Rev. Lett.* **2019**, *122*, 225701–.